

Evaluation of the WRF physical parameterisations for Typhoon rainstorm simulation in southeast coast of China



Jiyang Tian^{a,b}, Ronghua Liu^{a,b,*}, Liuqian Ding^a, Liang Guo^{a,b}, Qi Liu^{a,b}

^a China Institute of Water Resources and Hydropower Research, No.1 Fuxing Road, Haidian District, Beijing 100038, China

^b Research Center on Flood & Drought Disaster Reduction of the Ministry of Water Resources, No.1 Fuxing Road, Haidian District, Beijing 100038, China

ARTICLE INFO

Keywords:

Numerical rainfall simulation
WRF model
Physical parameterisations
Typhoon rainstorm
Rainfall evaluation statistics

ABSTRACT

Due to easily causing severe disasters in mountainous areas, typhoon rainfall forecast with numerical weather prediction (NWP) system plays an important role for meteorological and hydrological use. In order to investigate the applicability of physical parameterisations for typhoon rainstorms, thirty-six physical parameterisation combinations are designed by three microphysics (Lin, WSM6 and WDM6), three pairs of longwave/shortwave radiations (RRTM/Dudhia, RRTMG/RRTMG and CAM/CAM) and four cumulus parameterisations (KF, BMJ, GD and Grell 3D). The Weather Research and Forecasting (WRF) model is used to simulate the three representative typhoon storm events occurred in southeast coast of China and the rainfall simulations in Meixi catchment are evaluated. Not only for the individual parameterisation but also for the parameterisation combination, WSM6, RRTMG/RRTMG and KF outperform the other physical parameterisation as a whole. The WRF model has poor capability in simulating the rainfall caused by strong convection, and the storm events with uneven distributed rainfall tend to have worse rainfall simulation in space and time dimensions. The findings provide references for choosing the physical parameterisation, which can help to obtain relatively reliable typhoon rainfall forecast and flood warning in catchment scale. The shortage of the NWP system and the solution for improve the rainfall simulation are also put forward.

1. Introduction

The numerical weather prediction (NWP) system plays an important role in rainfall forecast for meteorological and hydrological use (Liguori et al., 2012). The Weather Research and Forecasting (WRF) model is a mesoscale NWP system used for atmospheric research, operational forecasting and dynamical downscaling of Global Climate Models (GCMs) (Evans et al., 2012; Tian et al., 2017a). Many cases indicate that the WRF model has good performance on the simulation of main meteorological elements, such as temperature, humidity, wind and pressure (Sharma et al., 2017; Ratnam et al., 2017; Hutchison et al., 2017). However, due to the complex formation mechanism and strong spatiotemporal heterogeneity, rainfall is still one of the most difficult variables to predict (Maussion et al., 2011; Liu et al., 2012; Avolio and Federico, 2018).

In order to accommodate the different synoptic situations, different physical parameterisations in WRF model can be combined in any way. From simple and efficient, to sophisticated and more computationally costly, physical parameterisation options have significant influences on rainfall simulations, not only for rainfall magnitude and duration, but

also for spatial and temporal distribution of the rainfall (Mohan et al., 2018; Li et al., 2020; Otieno et al., 2019). As the precondition of hydrological forecast, accurate rainfall simulation can prevent great losses effectively caused by flood, especially in the region where heavy rainfall and severe flood events occur frequently (Patel et al., 2019). If accurate forecasted rainfall are obtained, more counter measures can be proposed before the flood occurs. However, many studies indicate that the option of physical parameterisation is still worth to investigate to obtain relatively reliable rainfall simulation in different regions and different climatic conditions (Gómez-Navarro et al., 2015; Khain et al., 2016; Tian et al., 2017b).

Typhoon rainstorm is one of the most terrible natural disasters and always causes economical loss and casualties in southeast coast of China (Shen et al., 2017; Liu et al., 2018). Due to the influence of factors such as the steering flow intensity and simultaneous presence multiple storms developed from a variety of synoptic and mesoscale systems, the number of Typhoon with heavy rainfall and strong wind is staying at a high level in southeast coast of China (Mao and Wu, 2008; Potty et al., 2012). Fujian province located between Central Mountains in Taiwan and Wuyi Mountains suffers heavy rainfall and severe flood

* Corresponding author at: China Institute of Water Resources and Hydropower Research, No.1 Fuxing Road, Haidian District, Beijing 100038, China.
E-mail addresses: tjyshd@126.com (J. Tian), liurh@iwhr.com (R. Liu), dinglq@iwhr.com (L. Ding), guo@iwhr.com (L. Guo), liuqi@iwhr.com (Q. Liu).

caused by typhoon. Although the sensitivity studies of different physical parameterisations for typhoon rainstorm have been carried out in some regions, the selection remains inconclusive in different regions (Liu et al., 2013; Hsiao et al., 2013). The impact analysis of the rainfall causes and different typhoon stages on physical parameterisation choice is insufficient and unsystematic. In addition, different kinds of physical parameterisations are interrelated and interact on each other. The performance of the WRF model cannot be uniquely attributed to a single physical parameterisation but rather to the combination.

Microphysics, radiation and cumulus parameterisation are mostly discussed as the main influencing factors for rainfall simulation (Ferreira et al., 2014; Tang et al., 2019). Microphysics mainly influences the water phase transformation with the latent heat release and adsorption. Purdue-Lin (Lin), WRF Single-Moment 6 (WSM6) and WRF Double-Moment 6 (WDM6) can all describe the microphysics processes among six classes of hydrometeors: graupel, water vapor, cloud water, cloud ice, rain and snow (Lin et al., 1983; Hong et al., 2006; Lim and Hong, 2010). The three microphysics parameterisations are suitable for the complex weather simulation with high resolution.

Longwave/shortwave radiation parameterisations express the radiation propagation in the atmosphere, which play an important role in energy absorption, conversion and transmission, especially for the water phase transformation and rainfall formation (Ji et al., 2016). Rapid Radiative Transfer Model (RRTM) for longwave and Dudhia for shortwave are used frequently in any weather conditions. The RRTM for application to GCMs (RRTMG) with a reduced set of g-points optimisation method is more versatile than RRTM (Yuan et al., 2011). The National Center for Atmospheric Research (NCAR) Community Atmosphere Model (CAM) is able to handle optical properties of several aerosol types and trace gases (Montornès et al., 2015).

Cumulus convection process with cloud generation and evolution has close relationship with rainfall process. Cumulus parameterisations, such as Kain-Fritsch (KF), Betts-Miller-Janjić (BMJ), Grell-Devenyi (GD), Grell 3D, have been compared for rainfall simulation in East Asia (Cai et al., 2018). Preliminary results show that KF employs a simple cloud model and may enhance moisture convergence (Kain, 2004). BMJ performs well for the deep convection due to the objective description for vertical instabilities in moisture and temperature (Janjić, 2000). GD and Grell 3D are suitable for the NWP system with high-resolution (Grell and Freitas, 2014). Grell 3D, considering the convection effect between neighbored grids, is an improved version of GD. Both of them

apply to most convection conditions as using ensemble method within multiple cumulus parameterisations and variants (Madala et al., 2014).

One medium sized catchment, Meixi with an area nearly 1000 km², is chosen as the study area, which is located in the middle reach of Minjiang and representative in terms of climate and topography at Fujian province. It is crucially important for Fujian province to obtain accurate rainfall prediction. The aim of this study is to provide guidance for the selection of physical parameterisations in southeast coast of China, which can be used to predict typhoon rainstorms with high resolution at catchment scale. Three typhoon storm events occurred over Meixi catchment are selected with regard to different causes and different stages. The 36 combinations of physical parameterisations, including 3 microphysics parameterisations, 3 long/short radiation parameterisations and 4 cumulus parameterisations, are designed for the WRF model to regenerate the typhoon rainstorms. The rainfall simulations are evaluated comprehensively with total amounts and spatiotemporal distributions. The performances of physical parameterisations are also analysed in physical mechanism.

2. Study area and events

The Meixi catchment is located in the middle reach of Minjiang in southeast coast of China with humid climatic condition. The drainage area of the mountainous catchment (from lat 25°50' to lat 26°20'N and from long 118°30' to long 118°55'E) is 956 km², and there are 8 rain gauges in Meixi catchment (Fig. 1). The main stream with 78.6 km length flows into Minjiang at Xikou. The average annual rainfall is approximately 1560 mm in Meixi catchment and most heavy rainfalls are caused by typhoon generated in Western Pacific. Since 1949, the flood disasters have ravaged the Meixi catchment more than 20 times. The most destructive flood with the peak flow 4710 m³/s occurs on 9 July, 2016 and cause many casualties and huge economic losses. Accurate rainfall forecasts appear to be particularly important to avoid enormous losses caused by floods in Meixi catchment.

The representative typhoon storm events, including Saola, Hagibis and Nepartak, are chosen to investigate the applicability of physical parameterisations in Meixi catchment (Fig. 2). Saola was formed on July 28, 2012 and strengthened to typhoon on July 30. The typhoon gradually weakened after landing Taiwan on August 2 and landed second time on August 3 at Fuding, Fujian. With a slow moving speed, typhoon Saola weakened into a tropical storm at Jiangxi. Multiple

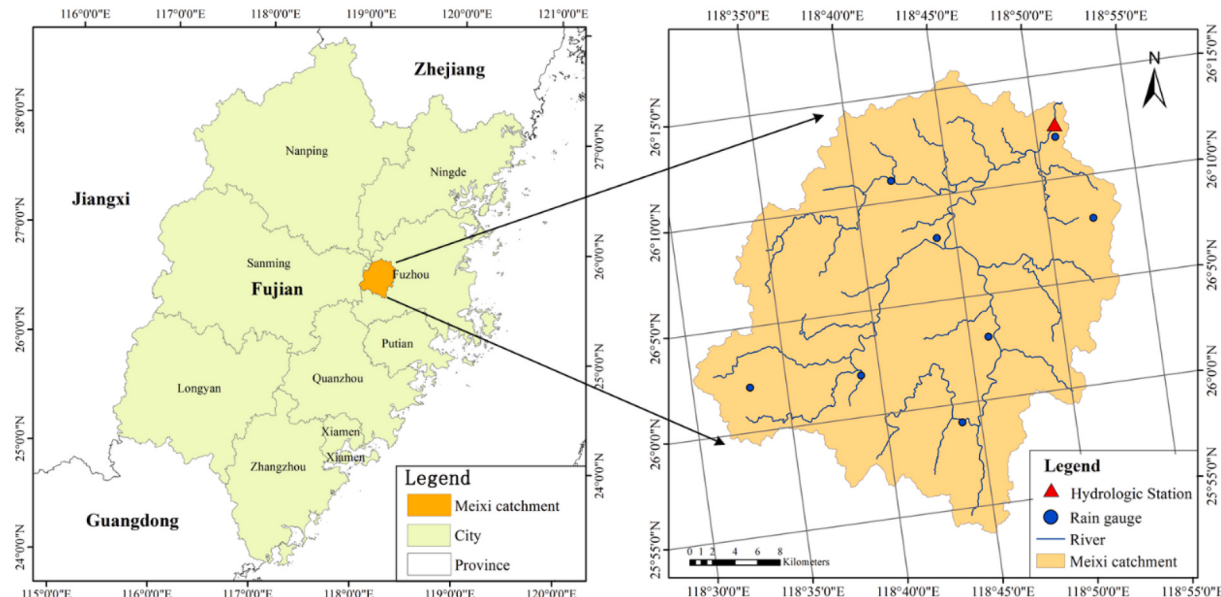


Fig. 1. The location of the Meixi catchment with eight rain gauges and one hydrologic station.

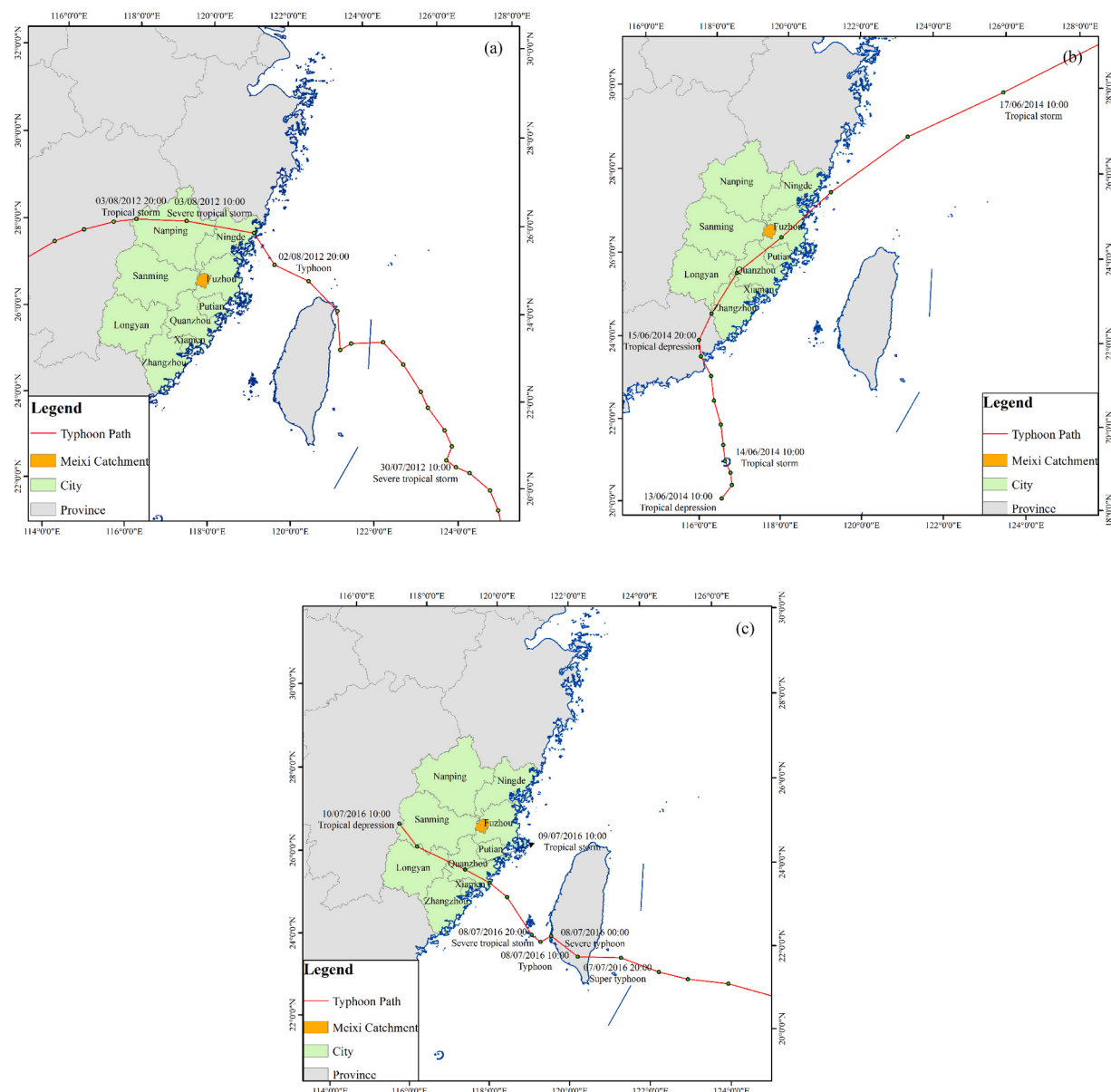


Fig. 2. The processes of three typhoon storms: (a) for Saola, (b) for Hagibis and (c) for Nepartak.

Table 1

Characteristics of the three typhoon storm events selected from Meixi catchment.

Event ID	Typhoon	Storm start time (UTC + 8)	Storm end time (UTC + 8)	24-h accumulated rainfall (mm)
I	Saola	03/08/2012 00:00	04/08/2012 00:00	84
II	Hagibis	17/06/2014 21:00	18/06/2014 21:00	66
III	Nepartak	08/07/2016 18:00	09/07/2016 18:00	242

factors, such as the north cold air and typhoon Damrey in the north, affected typhoon Saola and the rainfall formation condition. Although typhoon Saola brought heavy rain that affected a wider range over a long time period, the strongest vertical motion and upper level divergence were found at northern Sanming rather than Meixi catchment. According to the typhoon track, Saola never had a direct impact on Meixi catchment. Therefore, the accumulated 24-h rainfall for the whole catchment was only 84 mm.

Hagibis was intensified into a strong tropical storm over the South China Sea on June 14, 2014. Typhoon Hagibis moved toward north direction and landed in Shantou, Guangdong on June 15, 2014. Due to

the fast-moving speed, the southern Fujian was influenced by the typhoon Hagibis on the same day. However, typhoon Hagibis weakened into a tropical depression during moving through Fujian. Until June 17, tropical depression left northeastern Fujian and strengthened to tropical storm in the East China Sea. During this period, upward motion strengthened and moisture flux increased, which made formation conditions for the rainfall generation in Meixi catchment. The accumulated 24-h rainfall was 66 mm from 06/17 21:00 to 06/18 21:00.

A low-pressure zone emerged from the south of Guam on June 30, 2016, and strengthened to tropical storm named Nepartak in just a few days. Typhoon Nepartak made landfall over Taiwan on July 8 and

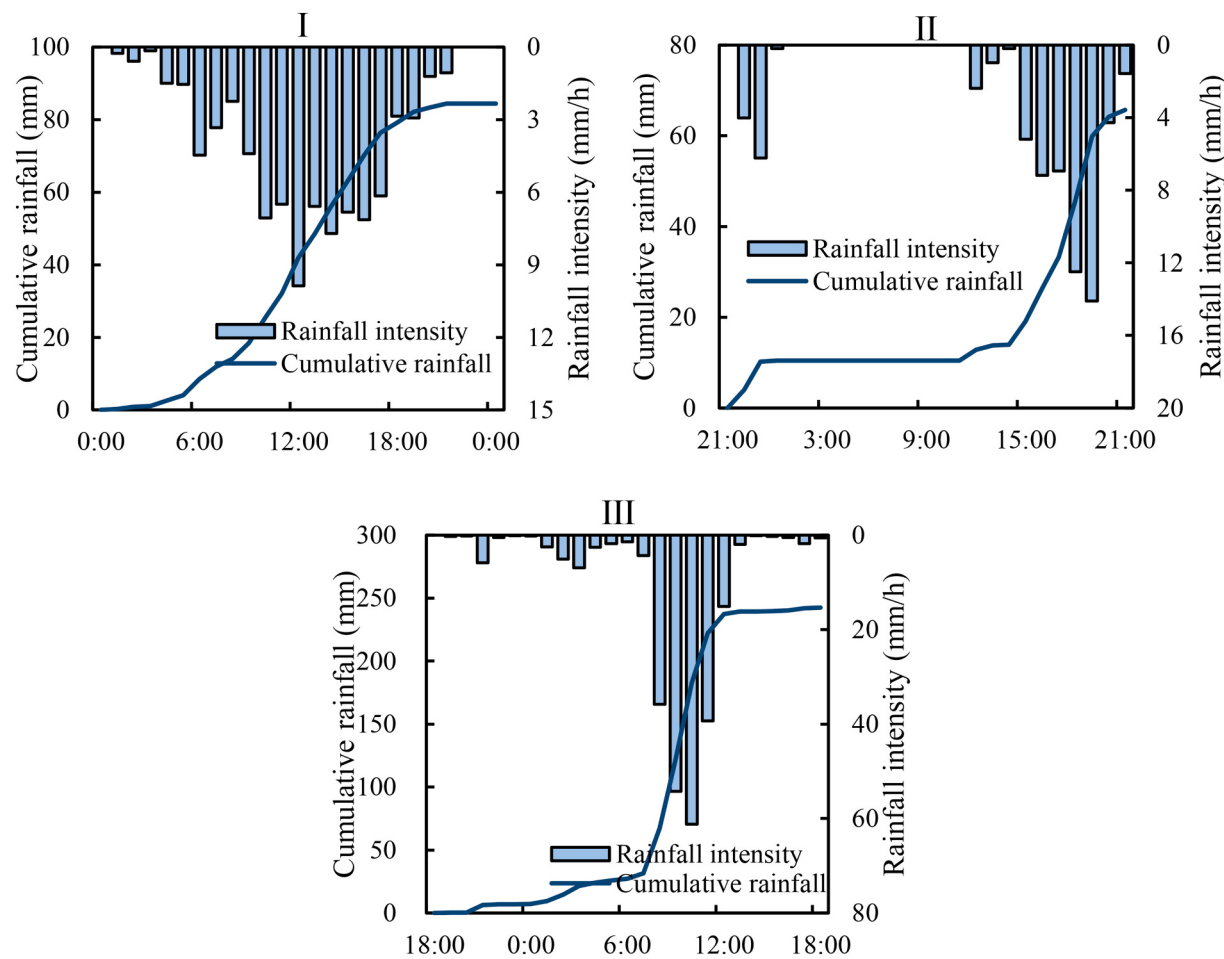


Fig. 3. Rainfall processes of the three typhoon events.

reached Fujian the next day. The convective cloud clusters enhanced at Putian and moved toward the northwest. On July 9, typhoon Neptak reached its peak intensity and influenced Meixi catchment directly. Instability stratification in coastal areas was activated by the interaction between typhoon Neptak and cold vortex. The invasion of cold air caused a forced lift and strengthened the convection of mesoscale spiral rainband. Unstable energy releasing is one of the most important factors leading to heavy rainfall.

The Meixi catchment is outside the main impact areas of typhoon Saola, whereas typhoon Hagibis has weaken significantly by the time it arrives at Meixi catchment. Only typhoon Neptak passes through Meixi catchment as the prosperity of rain cluster and impacts the study area directly. Three different rainfall storms are shown in Table 1 and Fig. 3. Event I has a relatively even rainfall distribution both in space and time across Meixi catchment with a 24-h accumulation of 84 mm. Although the rainfall accumulation of Event II (66 mm) is less than Event I, the rainfall happens with a very high intensity in a short period. Event III is an extreme case with a 24-h accumulation of 242 mm, and the rainfall is uneven in spatiotemporal distribution.

3. WRF model and evaluation statistics

3.1. WRF model and configurations

The numerical simulations for three rainfall storm events are conducted with the WRF model in version 4.0. The detailed descriptions of the WRF model can be found at the web site (<https://www2.mmm.ucar.edu/wrf/users/>). The formation, development and extinction of typhoon storms always range over a wide field, exactly as the Fig. 2

shown. However, the area of Meixi catchment is only 956 km², which is much smaller than the scale of the typhoon process. In order to solve the problem of scale matching and improve the computation efficiency, three nested domains are set with the ratio of 1:3. Three model domains with two-way nesting are set with grid spacings of 4 km, 12 km and 36 km. The innermost domain completely covers the Meixi catchment. The coverage set of outmost domain takes into consideration both large scale synoptic system and topographic effect (Chen et al., 2017). The grid numbers for the nested domain sizes are 100 × 100 for Dom 1, 210 × 210 for Dom 2 and 300 × 300 for Dom 3 (Fig. 4). The top level is set at 50 hPa for all domains, which have 40 vertical pressure levels. Many studies use the NCEP Final (FNL) Operational Global Analysis data to simulate the historical rainstorms for evaluating the physical parameterisations, because the boundary conditions from FNL are closer to actual atmospheric conditions than the forecasts. (Zhang et al., 2011; Sun et al., 2015). In this study, FNL with 1° × 1° grids are used to provide the initial and lateral boundary conditions for the WRF model. In order to develop the smaller scale convective features, a spin-up period of 12 h is conducive to obtain more accurate rainfall simulation with high spatial resolution (Sun and Wang, 2013; Fierro et al., 2013).

As discussed in the Introduction, 36 physical parameterisation combinations (Table 2) are designed by three microphysics (Lin, WSM6 and WDM6), three pairs of longwave/shortwave radiations (RRTM/Dudhia, RRTMG/RRTMG and CAM/CAM) and four cumulus parameterisations (KF, BMJ, GD and Grell 3D). Due to frequently and widely apply for rainfall simulation, the Yonsei University (YSU) is used as the planetary boundary layer (PBL) and Noah is used as land-surface model (LSM) (Ahsan and Khan, 2013; Srivastava et al., 2015).

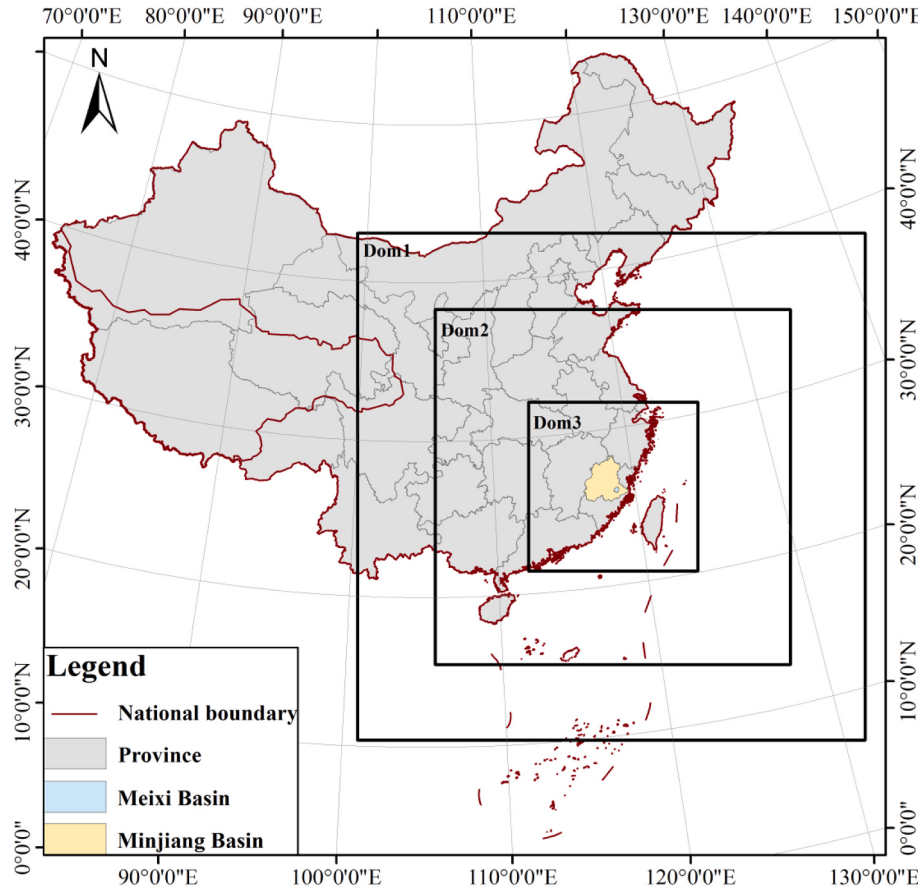


Fig. 4. The nested domains of WRF model for Meixi catchment.

3.2. Rainfall evaluation statistics

In order to evaluate the accuracy of rainfall simulation comprehensively, the relative error (*RE*) for the total rainfall amount evaluation is shown as follows (Mohapatra et al., 2017):

$$RE = \frac{P' - P}{P} \times 100\% \quad (1)$$

where P' is the simulation of 24-h accumulated areal rainfall, which is averaged from all grids inside the study area; and P is the observation of 24-h accumulated areal rainfall, which is calculated by the Thiessen polygon method with observations of the rain gauges (Sivapalan and Blöschl, 1998).

The critical success index (*CSI*) and modified root mean square error (m -RMSE) for spatiotemporal patterns of the rainfall simulation are expressed by Eqs. (2)–(3) (Tian et al., 2017b). m -RMSE is defined as the ratio of root mean square error (*RMSE*) to the mean values of the corresponding observations.

$$CSI = \frac{1}{N} \sum_{i=1}^N \frac{NA_i}{NA_i + NB_i + NC_i} \quad (2)$$

$$m - RMSE = \frac{\sqrt{\frac{1}{M} \sum_{j=1}^M (P'_j - P_j)^2}}{\frac{1}{M} \sum_{j=1}^M P_j} \quad (3)$$

For spatial dimension evaluation, NA , NB and NC at each hour ($i = 1$ h) are calculated by comparing the rainfall simulations with observations at the rain gauge locations as shown in Table 3, and N ($N = 24$ h) is the duration of the storm. For temporal dimension

evaluation, the three indices in Table 3 are calculated based on the time series data obtained for the simulated and observed areal rainfall at each rain gauge i , and this time N ($N = 8$) refers to the number of the total number of rain gauges in Meixi catchment. The perfect score of *CSI* is 1.

For spatial dimension evaluation, P'_j and P_j are the simulation and observation of 24-h accumulated rainfall at rain gauge j . M ($M = 8$) is the total number of rain gauges. For temporal dimension evaluation, P'_j and P_j are the areal rainfall simulation and observation at each time j ($j = 1$ h). M ($M = 24$ h) represents the total number of time steps. The perfect score of m -RMSE is 0.

4. Results

4.1. Evaluation of the accumulated areal rainfall simulation

Thirty-six rainfall simulations for each storm event are obtained by the WRF model to evaluate the performance of the thirty-six physical parameterisation combinations. Table 4 shows the *RE* values of rainfall accumulation for three different storm events, and thirty-six parameterisation schemes are also ranked based on *RE* values. Experiment 13 has the best performance in the thirty-six schemes for all the three storm events and the *RE* value is only 0.88% for event I. Comparing with other experiments, experiments 10–18 perform well for the three storm events and mostly rank in the top 10. According to *RE* values, the simulations of the WRF model are better for event I than event II and III, and event III is failed to be regenerated especially for hydrological use.

Table 5 shows the average relative error (*ARE*) of the rainfall accumulation for three storm events. The *ARE* for a certain physical parameterisation is calculated by the *RE* values of different schemes, which contain the physical parameterisation. For example, the *ARE*

Table 2

Thirty-six physical parameterisation combinations for rainfall simulation experiments.

Experiment ID	Microphysics	long/short wave radiation	Cumulus parameterisation
1	WSM6	RRTM/Dudhia	BMJ
2	WDM6	RRTM/Dudhia	BMJ
3	Lin	RRTM/Dudhia	BMJ
4	WSM6	RRTMG/RRTMG	BMJ
5	WDM6	RRTMG/RRTMG	BMJ
6	Lin	RRTMG/RRTMG	BMJ
7	WSM6	CAM/CAM	BMJ
8	WDM6	CAM/CAM	BMJ
9	Lin	CAM/CAM	BMJ
10	WSM6	RRTM/Dudhia	KF
11	WDM6	RRTM/Dudhia	KF
12	Lin	RRTM/Dudhia	KF
13	WSM6	RRTMG/RRTMG	KF
14	WDM6	RRTMG/RRTMG	KF
15	Lin	RRTMG/RRTMG	KF
16	WSM6	CAM/CAM	KF
17	WDM6	CAM/CAM	KF
18	Lin	CAM/CAM	KF
19	WSM6	RRTM/Dudhia	G3D
20	WDM6	RRTM/Dudhia	G3D
21	Lin	RRTM/Dudhia	G3D
22	WSM6	RRTMG/RRTMG	G3D
23	WDM6	RRTMG/RRTMG	G3D
24	Lin	RRTMG/RRTMG	G3D
25	WSM6	CAM/CAM	G3D
26	WDM6	CAM/CAM	G3D
27	Lin	CAM/CAM	G3D
28	WSM6	RRTM/Dudhia	GD
29	WDM6	RRTM/Dudhia	GD
30	Lin	RRTM/Dudhia	GD
31	WSM6	RRTMG/RRTMG	GD
32	WDM6	RRTMG/RRTMG	GD
33	Lin	RRTMG/RRTMG	GD
34	WSM6	CAM/CAM	GD
35	WDM6	CAM/CAM	GD
36	Lin	CAM/CAM	GD

Table 3

Rain-no rain contingency table for the rainfall simulation against observation.

WRF rainfall simulation/observation	Rain	No rain (< 0.1 mm/h)
Rain	NA (hit)	NB (false alarm)
No rain (< 0.1 mm/h)	NC (failure)	/

value of WSM6 for Event I (9.22%) represents the average performance of the WSM6-contained Experiments 1 (13.27%), 4 (13.57%), 7 (13.40%), 10 (6.28%), 13 (0.88%), 16 (6.70%), 19 (20.73%), 22 (17.34%), 25 (21.00%), 28 (6.32%), 31 (5.96%) and 34 (8.06%). In the three microphysics, WSM6 is the best choice for all the three storm events. For the three pairs of long/short wave radiation parameterisations, RRTMG/RRTMG perform best for all the three storm events, while CAM/CAM consistently perform the worst. KF with the minimum AREs has the best performance among the four cumulus parameterisations, whereas G3D always performs worst. As a whole, WSM6 for microphysics, RRTMG/RRTMG for radiation parameterisation and KF for cumulus parameterisation with the lowest ARE values, indicate that the combination of the three kinds of physical parameterisations lead to the best performance on rainfall accumulation in the Meixi catchment. The result is consistent with the finding that experiment 13 is the best choice among the thirty-six physical parameterisation combinations.

Table 4

RE values (%) of the rainfall accumulation for three storm events.

Experiment ID	Event I	Event II	Event III
1	13.27 (22)	-65.23 (29)	-80.18 (11)
2	14.43 (25)	-64.95 (27)	-83.81 (29)
3	11.60 (20)	-56.69 (14)	-83.19 (25)
4	13.57 (24)	-65.39 (30)	-80.81 (14)
5	14.75 (28)	-65.63 (31)	-84.62 (34)
6	11.88 (21)	-56.45 (13)	-84.01 (31)
7	13.40 (23)	-64.55 (26)	-79.89 (10)
8	14.71 (27)	-64.05 (25)	-83.03 (24)
9	11.19 (19)	-58.13 (22)	-82.91 (23)
10	6.28 (13)	-37.25 (8)	-74.91 (2)
11	5.16 (7)	-37.83 (9)	-78.48 (8)
12	2.22 (4)	-26.90 (2)	-75.81 (5)
13	0.88 (1)	-24.32 (1)	-73.47 (1)
14	2.31 (5)	-35.58 (5)	-78.43 (7)
15	1.32 (2)	-27.29 (3)	-75.35 (4)
16	6.70 (15)	-35.83 (6)	-75.34 (3)
17	5.92 (11)	-36.01 (7)	-80.32 (12)
18	1.67 (3)	-32.53 (4)	-78.40 (6)
19	20.73 (35)	-68.51 (36)	-82.07 (21)
20	20.65 (34)	-68.30 (35)	-83.89 (30)
21	19.55 (33)	-60.31 (23)	-80.90 (15)
22	17.34 (30)	-65.82 (32)	-81.00 (16)
23	14.57 (26)	-65.05 (28)	-80.72 (13)
24	15.55 (29)	-57.64 (20)	-79.84 (9)
25	21.00 (36)	-66.54 (33)	-83.28 (26)
26	19.48 (32)	-66.88 (34)	-85.78 (35)
27	17.34 (30)	-61.82 (24)	-81.78 (18)
28	6.32 (14)	-57.15 (17)	-82.11 (22)
29	5.78 (10)	-57.46 (18)	-83.61 (27)
30	5.06 (6)	-47.02 (10)	-82.06 (20)
31	5.96 (12)	-57.05 (16)	-81.94 (19)
32	5.32 (9)	-57.52 (19)	-83.62 (28)
33	5.31 (8)	-48.08 (11)	-81.72 (17)
34	8.06 (18)	-57.04 (15)	-84.30 (32)
35	6.85 (16)	-58.02 (21)	-86.05 (36)
36	7.91 (17)	-50.99 (12)	-84.60 (33)

Rankings of the different parameterisation schemes based on RE (%) are shown in () .

4.2. Evaluation of the spatiotemporal patterns for rainfall simulation

In addition to the accumulated areal rainfall, the spatiotemporal distributions of rainfall also have significant effect on flood process for the medium sized catchment. The *CSI* and *m-RMSE* are used to evaluate the spatiotemporal patterns of rainfall simulation for the thirty-six parameterisation schemes.

4.2.1. Evaluation of the spatial distribution for rainfall simulation

Table 6 shows the *CSI* and *m-RMSE* for spatial distribution of rainfall. The parameterisation schemes are also ranked according to the *CSI* and *m-RMSE*. Different physical parameterisation combinations have different performance for the three storm events. The highest *CSI* can be found in experiment 13 for event I and II, while experiment 15 performs best in the 36 experiments for event III. Experiment 15 has the lowest *m-RMSE* for event I and III, whereas experiment 13 is the best choice for event III. Considering the rankings of physical parameterisation combinations for the three storm events as a whole, experiment 13 has a stable performance and ranks in the top 3 not only based on *CSI* but also according to *m-RMSE*. Same as the result shown in [Section 4.1](#), experiments 10–18 also perform well for the three storm events and mostly rank in the top 10. The spatial distribution of the rainfall simulations and observations for the three storm events are shown in [Figs. 5–7](#). Based on *CSI*, the ranking of the WRF model performance in simulating spatial distribution of rainfall is event I > event III > event II. From the [Figs. 5–7](#), the spatial distribution of observed rainfall

Table 5

ARE values (%) of the physical parameterisations for three storm events.

Physical parameterisation		Event I	Event II	Event III
Microphysics	WSM6	9.22	-48.65	-79.94
	WDM6	10.83	-56.44	-82.70
	Lin	11.13	-55.39	-80.88
Longwave/shortwave radiation	RRTM/Dudhia	9.38	-53.97	-80.92
	RRRTMG/RRRTMG	8.20	-52.15	-80.46
	CAM/CAM	10.98	-54.37	-82.14
Cumulus parameterisations	BMJ	13.20	-62.34	-82.49
	KF	3.61	-32.62	-76.72
	G3D	18.47	-64.54	-82.14
	GD	6.29	-54.48	-83.33

for event II is more uneven than event I and III, which makes the WRF model difficult to capture the falling area. In contrast, the WRF model performs well for event I with even spatial distribution. Due to the failure of reproducing the rainfall magnitude, event III has the highest *m-RMSE* in the three storm events.

The average value of *CSI* and the average value of *m-RMSE* for spatial distribution of rainfall are used to further compare different physical parameterisations (shown in Table 7). The calculation method of average values for *CSI* and *m-RMSE* is similar with *ARE* calculation. The results show that WSM6 with highest *CSI* and lowest *m-RMSE*

performs better than WDM6 and Lin. RRTMG/RRTMG is the best combination for longwave/shortwave radiation parameterisation, and KF is the best choice in the four cumulus parameterisations. Comparing the *CSIs* and the *m-RMSEs* for three kinds of physical parameterisations, cumulus parameterisation has a higher effect on the rainfall spatial distribution simulation than microphysics and radiation parameterisations.

4.2.2. Evaluation of the temporal distribution for rainfall simulation

The experiments are ranked based on the *CSI* and *m-RMSE*, which are also calculated for temporal distribution of rainfall (shown in Table 8). Comparing with the evaluation indices for spatial distribution of rainfall, the *CSI* is lower and the *m-RMSE* is higher in Table 8, which indicates that the WRF model performs worse in simulating the rainfall process in temporal dimension. The main reason is that the rainfall is more variable in time than in space. The highest *CSI* can be found in experiment 13 for event I, in experiment 15 for event II and in experiment 21 for event III. Experiments 16, 13 and 14 have the lowest *m-RMSE* for event I, II and III respectively. Although it is difficult to point out which physical parameterisation combination is the most suitable for simulating the temporal distribution of rainfall in Meixi catchment, considering the rankings of physical parameterisation combinations for the three storm events as a whole, experiment 13 is the right choice. Because experiment 13 has the stable performance and ranks in the top 6 not only based on the *CSI* but also according to the *m-RMSE*.

Table 6*CSI* and *m-RMSE* for spatial distribution of rainfall simulation.

Experiment ID	Event I		Event II		Event III	
	CSI	<i>m-RMSE</i>	CSI	<i>m-RMSE</i>	CSI	<i>m-RMSE</i>
1	0.7362 (21)	0.1676 (19)	0.4377 (20)	0.8345 (30)	0.6128 (23)	0.8488 (19)
2	0.7350 (27)	0.1794 (25)	0.4531 (11)	0.8308 (28)	0.6140 (20)	0.8574 (23)
3	0.7361 (22)	0.1963 (31)	0.4222 (25)	0.7678 (21)	0.6106 (24)	0.8376 (14)
4	0.7356 (25)	0.1546 (13)	0.4229 (24)	0.7626 (19)	0.6189 (8)	0.8415 (17)
5	0.7448 (9)	0.1640 (18)	0.4428 (18)	0.8395 (34)	0.6146 (14)	0.8469 (18)
6	0.7359 (23)	0.1717 (22)	0.4324 (22)	0.8365 (32)	0.6049 (26)	0.8305 (13)
7	0.7358 (24)	0.1730 (23)	0.4503 (15)	0.7909 (23)	0.6157 (12)	0.8627 (27)
8	0.7349 (28)	0.1625 (17)	0.4074 (27)	0.8357 (31)	0.6137 (21)	0.8691 (31)
9	0.7353 (26)	0.1807 (26)	0.4351 (21)	0.8393 (33)	0.6137 (21)	0.8592 (24)
10	0.7491 (6)	0.1441 (6)	0.4614 (6)	0.5662 (8)	0.6338 (3)	0.7814 (5)
11	0.7449 (8)	0.1478 (9)	0.4561 (8)	0.5726 (9)	0.6180 (9)	0.8063 (7)
12	0.7468 (17)	0.1345 (2)	0.4716 (3)	0.5216 (1)	0.6146 (14)	0.7725 (4)
13	0.7582 (1)	0.1409 (3)	0.4879 (1)	0.5235 (2)	0.6353 (2)	0.7482 (1)
14	0.7454 (7)	0.1420 (4)	0.4675 (4)	0.5649 (7)	0.6180 (9)	0.7966 (6)
15	0.7538 (2)	0.1331 (1)	0.4842 (2)	0.5627 (6)	0.6483 (1)	0.7719 (3)
16	0.7534 (3)	0.1479 (10)	0.4601 (7)	0.5365 (4)	0.6321 (4)	0.7673 (2)
17	0.7411 (10)	0.1439 (5)	0.4557 (9)	0.5297 (3)	0.6275 (5)	0.8292 (12)
18	0.7504 (4)	0.1461 (7)	0.4628 (5)	0.5368 (5)	0.6230 (6)	0.8106 (8)
19	0.7344 (31)	0.1960 (30)	0.4103 (26)	0.7814 (22)	0.5301 (33)	0.8599 (25)
20	0.7341 (33)	0.2095 (35)	0.3571 (34)	0.8413 (35)	0.5109 (36)	0.8850 (36)
21	0.7342 (32)	0.1956 (29)	0.3470 (36)	0.8451 (36)	0.5310 (32)	0.8748 (32)
22	0.7345 (30)	0.2029 (34)	0.3632 (33)	0.8216 (26)	0.5947 (28)	0.8623 (26)
23	0.7492 (5)	0.2216 (36)	0.3476 (35)	0.8149 (25)	0.5190 (35)	0.8778 (35)
24	0.7348 (29)	0.1986 (32)	0.3870 (30)	0.7649 (20)	0.5708 (29)	0.8760 (33)
25	0.7338 (36)	0.1879 (27)	0.4071 (28)	0.8228 (27)	0.5444 (30)	0.8526 (21)
26	0.7337 (35)	0.1996 (33)	0.3684 (32)	0.8311 (29)	0.5220 (34)	0.8643 (29)
27	0.7340 (34)	0.1906 (28)	0.3788 (31)	0.7951 (24)	0.5383 (31)	0.8649 (30)
28	0.7371 (15)	0.1547 (14)	0.3916 (29)	0.7197 (11)	0.6145 (16)	0.8531 (22)
29	0.7368 (17)	0.1578 (15)	0.4423 (19)	0.7481 (15)	0.6144 (17)	0.8516 (20)
30	0.7365 (20)	0.1595 (16)	0.4512 (14)	0.7540 (17)	0.6142 (19)	0.8280 (11)
31	0.7409 (11)	0.1539 (12)	0.4543 (10)	0.7327 (12)	0.6154 (13)	0.8391 (15)
32	0.7377 (14)	0.1679 (20)	0.4494 (16)	0.7360 (13)	0.6206 (7)	0.8142 (9)
33	0.7398 (13)	0.1471 (8)	0.4494 (16)	0.6835 (10)	0.6143 (18)	0.8214 (10)
34	0.7401 (12)	0.1535 (11)	0.4525 (13)	0.7499 (16)	0.6028 (27)	0.8634 (28)
35	0.7469 (16)	0.1688 (21)	0.4308 (23)	0.7613 (18)	0.6175 (11)	0.8766 (34)
36	0.7366 (19)	0.1749 (24)	0.4530 (12)	0.7364 (14)	0.6086 (25)	0.8401 (16)

Rankings of the different parameterisation schemes based on *CSI* or *m-RMSE* are shown in ()�.

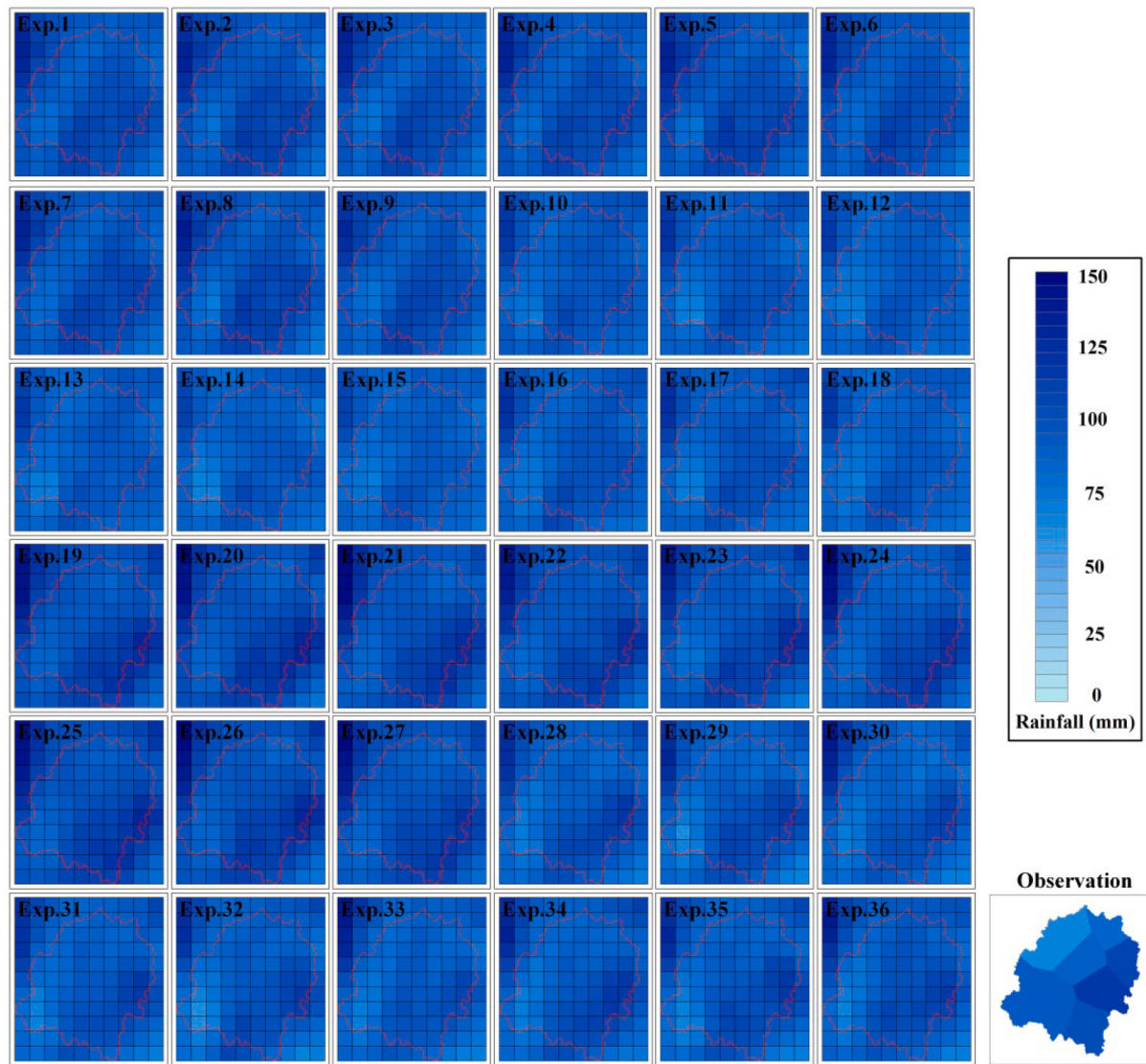


Fig. 5. Spatial distribution of the 36 rainfall simulations and the rainfall observation for Event I.

Figs. 8–10 show the simulated and observed rainfall processes with time series bars for the three storm events. According to the *CSI*, the ranking of the WRF model performance in simulating temporal distribution of rainfall is event I > event III > event II. Figs. 8–10 show the rainfall concentrated in only a few hours for storm event II and III, while the rainfall of storm event I is even in temporal dimension. The simulation of the WRF model becomes more difficult with the increase of temporal rainfall unevenness. Based on the *m-RMSE*, the ranking of the WRF model performance in simulating temporal distribution of rainfall is event I > event II > event III. Due to the failure of reproducing the rainfall magnitude, event III also has the highest *m-RMSE* in the three storm events.

The average value of *CSI* and the average value of *m-RMSE* for temporal distribution of rainfall are calculated to further compare different physical parameterisations (shown in Table 9). The results show that WSM6 with highest *CSI* and lowest *m-RMSE* performs better than WDM6 and Lin for event II and III. The WSM6 also has the highest *CSI* while WDM6 has the lowest *m-RMSE* for event I. For the three storm events, RRTMG/RRTMG is the best choice for longwave/shortwave radiation parameterisation, and KF performs best in the four cumulus parameterisations. Comparing the *CSIs* and the *m-RMSEs* for three kinds

of physical parameterisations, the same conclusion can be obtained as Section 4.2.1: cumulus parameterisation has a higher effect on the temporal distribution of rainfall simulation than other two kinds of physical parameterisations.

5. Discussion

Thirty-six physical parameterisation combinations are tested by the simulations of three storm events in both accumulated rainfall amount and spatiotemporal distributions. Although experiment 13 is generally the right choice for rainfall simulations in Meixi catchment, the *CSIs* and *m-RMSEs* indicate that experiment 13 is not always the best in the thirty-six physical parameterisation combinations for simulating the spatiotemporal rainfall distributions. Such as experiment 15 has the lowest *m-RMSE* for event I and highest *CSI* for event III in spatial dimension, while the lowest *m-RMSE* can be found in experiment 16 for event I and experiment 14 for event III. In order to reduce the rainfall forecasting uncertainties in operational applications, ensemble forecasting with different physical parameterisation combinations has become a conventional technique. Due to the stable and outstanding performance, experiments 13, 14, 15 and 16 can be used as physical

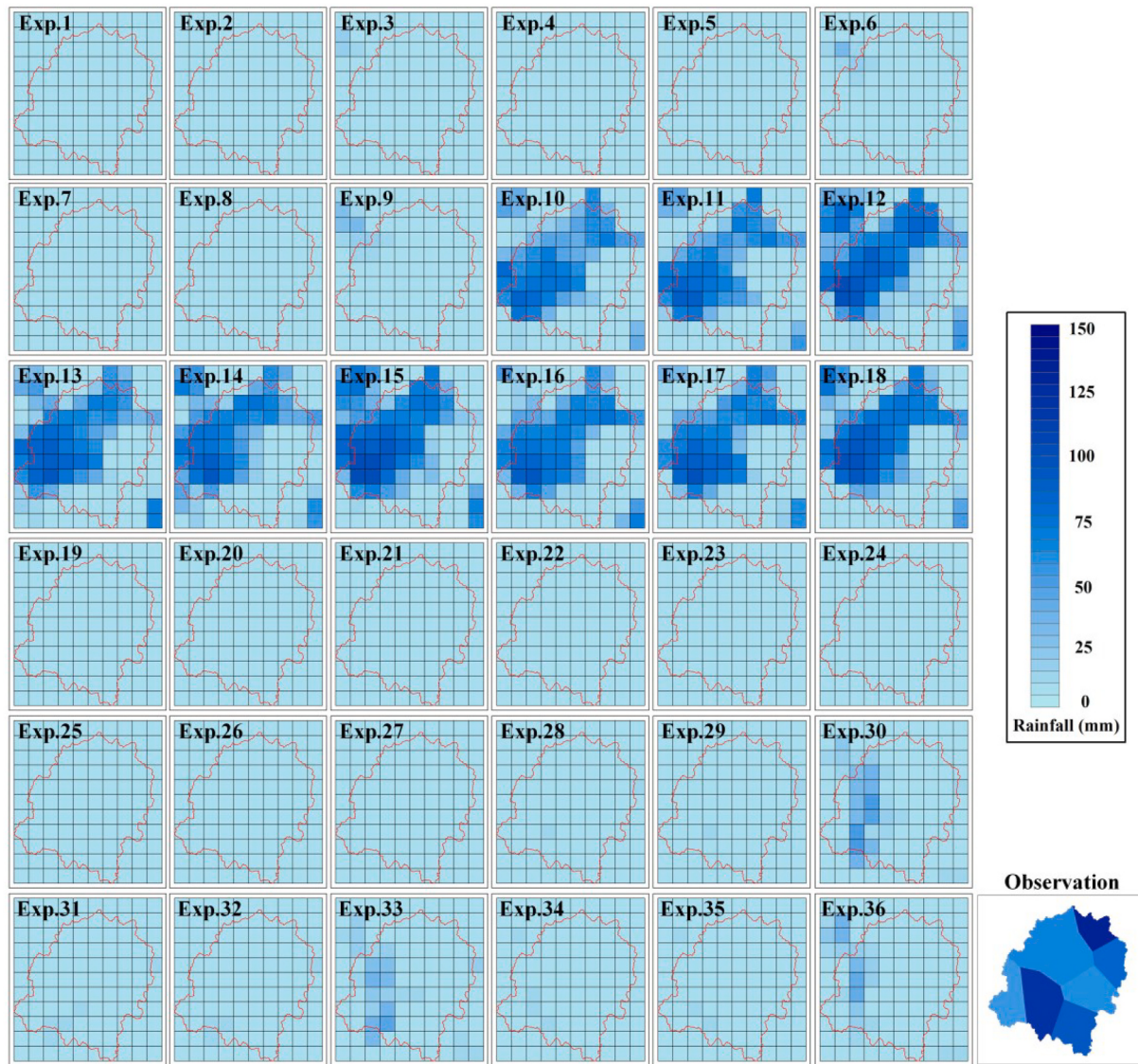


Fig. 6. Spatial distribution of the 36 rainfall simulations and the rainfall observation for Event II.

ensemble of the WRF model in Meixi catchment. The comprehensive evaluation method of the rainfall simulation in this study also provide reference for selecting physical parameterisation and generating physical ensemble of NWP system.

For the individual parameterisations, WSM6 for microphysics, RRTMG/RRTMG for longwave/shortwave radiation parameterisation and KF for cumulus parameterisation always perform better than other physical parameterisations in rainfall simulation. Although the three microphysics are similar, the state transformation of hydrometeor in falling process can be described with WSM6 rather than Lin, which can help WSM6 to improve the simulation accuracy for vertical profile of physical quantity. WDM6 has double-moment rain to investigate the aerosol effects on rainfall processes with the prognostic variables of cloud condensation nuclei (CCN), which make WDM6 tend to produce a large number of small raindrops rather than large raindrops (Duda et al., 2014). In southeast coast of China, the rainfall always has large raindrops especially during the typhoon storm events. That is the reason why WSM6 performs a little better than other two microphysics.

RRTMG/RRTMG with a reduced set of g-points optimization method has higher calculation efficiency than other two radiation

parameterisations. Additionally, RRTMG/RRTMG generally can reflect the influence of the cloud in different height layer and sub-grid scale, which helps to obtain the accuracy rainfall simulation in typhoon storm events with thick clouds and complex weather processes (Yuan et al., 2011). CAM always makes the ground temperature low, which goes against the development of upward movement (Zittis and Hadjinicolaou, 2017).

The choice of cumulus parameterisations has a greater impact on rainfall simulation than other two kinds of physical parameterisations. KF with the best performance utilises a simple cloud model to simulate moist up/down drafts and uses low-level vertical motion as a trigger function, thus it can provide better simulations of convective processes associated with thermodynamic vertical motion (Madala et al., 2014). BMJ can adjust instabilities in the environment by generating deep convection in tropics, while it is inapplicable to non-tropical environment and at small scales (Kerkhoven et al., 2005). GD and Grell 3D employs a large ensemble of closure assumptions and parameters to obtain the optimal value. The two cumulus parameterisations have wide applicability but weak pertinence.

Comparing with the scale of the study area, the driving data with

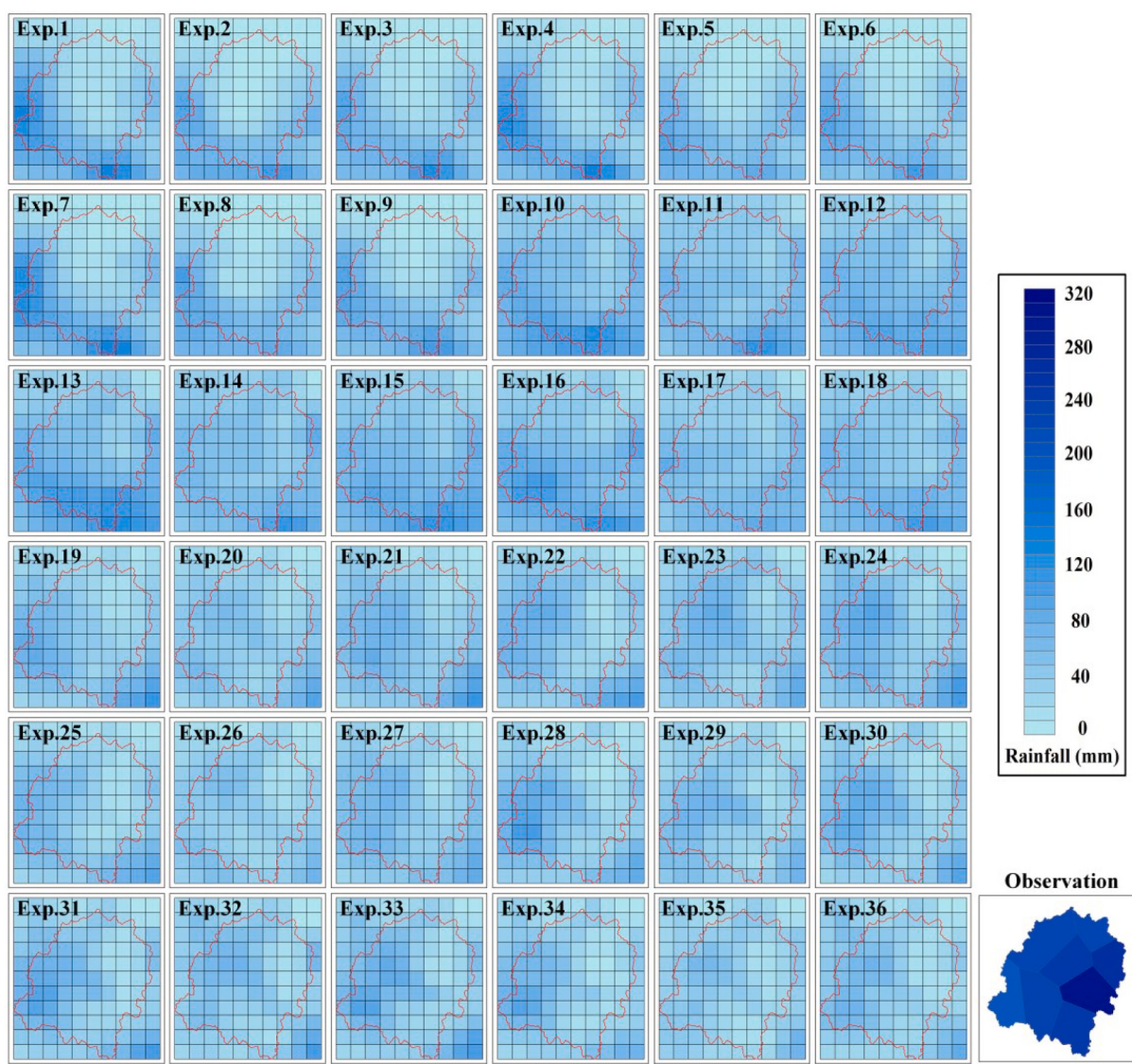


Fig. 7. Spatial distribution of the 36 rainfall simulations and the rainfall observation for Event III.

Table 7

The average value of *CSI* and the average value of *m-RMSE* for spatial distribution of rainfall simulation.

Physical parameterisation	Event I		Event II		Event III	
	<i>CSI</i>	<i>m-RMSE</i>	<i>CSI</i>	<i>m-RMSE</i>	<i>CSI</i>	<i>m-RMSE</i>
Microphysics	WSM6	0.7408	0.1648	0.4333	0.7202	0.6042
	WDM6	0.7403	0.1721	0.4231	0.7422	0.5925
	Lin	0.7395	0.1691	0.4312	0.7203	0.5994
Longwave/shortwave radiation	RRTM/Dudhia	0.7384	0.1702	0.4251	0.7319	0.5932
	RRTMG/RRTMG	0.7426	0.1665	0.4324	0.7203	0.6062
Cumulus parameterisations	CAM/CAM	0.7397	0.1691	0.4302	0.7304	0.5966
	BMJ	0.7366	0.1722	0.4338	0.8153	0.6132
	KF	0.7492	0.1423	0.4675	0.5461	0.6278
	G3D	0.7359	0.2003	0.3741	0.8131	0.5401
	GD	0.7392	0.1598	0.4416	0.7357	0.6136

$1^\circ \times 1^\circ$ grids seems to be a little rough. The deviation in the initial and lateral boundary condition is the main reason why the WRF model has weak ability to simulate the heavy rainfall with a short-time duration. Severe convection during typhoon process always occurs in mesoscale synoptic system and leads to heavy rainfall. The 4-h accumulated

rainfall from 8:00 to 12:00 reaches 190 mm for Event III and the storm center happens to be in Meixi catchment. It is a typical severe convection weather caused by typhoon. The horizontal scale of the general convection is no more than 300 km. Therefore, FNL with $1^\circ \times 1^\circ$ grids may be not suitable for the severe convection simulation in catchment

Table 8CSI and *m*-RMSE for temporal distribution of rainfall simulation.

Experiment ID	Event I		Event II		Event III	
	CSI	<i>m</i> -RMSE	CSI	<i>m</i> -RMSE	CSI	<i>m</i> -RMSE
1	0.7091 (14)	0.6425 (9)	0.3666 (27)	1.5715 (25)	0.5305 (31)	1.9295 (19)
2	0.6884 (24)	0.6587 (13)	0.3676 (26)	1.6349 (36)	0.4955 (36)	1.9372 (23)
3	0.6875 (30)	0.7131 (26)	0.3563 (31)	1.6322 (34)	0.5216 (33)	1.9308 (20)
4	0.7272 (9)	0.6438 (10)	0.3906 (14)	1.5583 (22)	0.5923 (25)	1.9223 (16)
5	0.6885 (23)	0.6355 (8)	0.3750 (20)	1.6326 (35)	0.5124 (34)	1.9191 (13)
6	0.6881 (26)	0.7168 (28)	0.3942 (10)	1.6313 (33)	0.5632 (29)	1.9329 (22)
7	0.6908 (20)	0.6725 (18)	0.3718 (25)	1.5768 (27)	0.5301 (32)	1.9522 (26)
8	0.6878 (27)	0.6674 (16)	0.3666 (27)	1.6294 (32)	0.5097 (35)	1.9557 (27)
9	0.6878 (27)	0.7213 (29)	0.3647 (29)	1.6161 (31)	0.5409 (30)	1.9465 (25)
10	0.7355 (6)	0.6219 (6)	0.3734 (23)	1.3075 (3)	0.6150 (7)	1.8924 (7)
11	0.7458 (3)	0.6166 (5)	0.3903 (15)	1.3027 (2)	0.6146 (10)	1.8920 (5)
12	0.7362 (5)	0.6520 (12)	0.3834 (17)	1.3526 (7)	0.6141 (11)	1.9021 (10)
13	0.7471 (1)	0.6018 (3)	0.4306 (2)	1.3001 (1)	0.6151 (6)	1.8845 (3)
14	0.7308 (7)	0.5973 (2)	0.4111 (5)	1.3105 (4)	0.6149 (8)	1.8734 (1)
15	0.7467 (2)	0.6317 (7)	0.4356 (1)	1.4217 (9)	0.6147 (9)	1.8811 (2)
16	0.7362 (4)	0.5924 (1)	0.4000 (7)	1.3434 (6)	0.6153 (5)	1.9020 (9)
17	0.7177 (12)	0.6076 (4)	0.3722 (24)	1.3252 (5)	0.6137 (12)	1.9185 (12)
18	0.7222 (11)	0.6449 (11)	0.3901 (16)	1.3663 (8)	0.6131 (13)	1.8943 (8)
19	0.6876 (29)	0.7060 (25)	0.3935 (11)	1.5998 (30)	0.6178 (3)	1.9932 (32)
20	0.6882 (25)	0.7053 (23)	0.3292 (36)	1.5952 (29)	0.5982 (22)	2.0018 (35)
21	0.6874 (32)	0.7285 (30)	0.3410 (33)	1.5471 (20)	0.6252 (1)	1.9962 (33)
22	0.6889 (22)	0.6934 (19)	0.3539 (32)	1.5648 (24)	0.6057 (16)	1.9929 (31)
23	0.6871 (33)	0.6996 (21)	0.3392 (34)	1.5541 (21)	0.5945 (23)	2.0018 (35)
24	0.6865 (36)	0.7369 (32)	0.3788 (19)	1.5427 (19)	0.6042 (18)	1.9920 (30)
25	0.6875 (30)	0.7293 (31)	0.3931 (12)	1.5593 (23)	0.6019 (20)	1.9865 (28)
26	0.6870 (34)	0.7425 (33)	0.3359 (35)	1.5843 (28)	0.6158 (4)	2.0011 (34)
27	0.6867 (35)	0.7476 (34)	0.3567 (30)	1.5718 (26)	0.5910 (26)	1.9897 (29)
28	0.7263 (10)	0.6723 (17)	0.4222 (3)	1.5352 (18)	0.6049 (17)	1.9275 (18)
29	0.6912 (18)	0.6991 (20)	0.3798 (18)	1.5223 (17)	0.5863 (27)	1.9325 (21)
30	0.6904 (21)	0.7600 (36)	0.3962 (9)	1.5124 (16)	0.5945 (23)	1.9178 (11)
31	0.7273 (8)	0.7053 (23)	0.3988 (8)	1.4348 (10)	0.6106 (14)	1.8875 (4)
32	0.6932 (17)	0.6657 (15)	0.3739 (21)	1.4520 (11)	0.6187 (2)	1.9205 (14)
33	0.6995 (15)	0.7532 (35)	0.4042 (6)	1.4548 (12)	0.5990 (21)	1.8923 (6)
34	0.7095 (13)	0.7031 (22)	0.3917 (13)	1.4714 (13)	0.6027 (19)	1.9268 (17)
35	0.6912 (18)	0.6644 (14)	0.4139 (4)	1.5030 (15)	0.5822 (28)	1.9413 (24)
36	0.6992 (16)	0.7131 (26)	0.3739 (21)	1.4770 (14)	0.6091 (15)	1.9216 (15)

Rankings of the different parameterisation schemes based on CSI or *m*-RMSE are shown in ()�.

scale. How to improve the simulation accuracy and reduce the uncertainties for rainfall simulation? Data assimilation using high-resolution local observation data is an efficient methods to correct the initial and lateral boundary conditions. Many studies indicate that radar data should be the right choice because of the high spatiotemporal resolution and good detection ability of severe convection (Shen et al., 2017).

Additionally, there are only 8 rain gauges in Meixi catchment, which means that only one rain gauge locates in an area of 125 km². It is the limitation of the study that the station density is much smaller than the grid size of the WRF model. In order to improve the results reliability, more ground observations should be used to evaluate the rainfall simulations with the constructions of rain gauges and X-band in the Meixi catchment.

6. Conclusions

Three representative typhoon storm events, including Saola, Hagibis and Nepartak, are chosen to be investigate the applicability of physical parameterisations in Meixi catchment in southeast coast of China. The FNL analysis data with 1° × 1° grids are used to provide the initial and lateral boundary conditions for the WRF model. Thirty-six physical parameterisation combinations are designed by three microphysics, three pairs of longwave/shortwave radiations and four cumulus parameterisations. The WRF outputs with 36 physical parameterisation combinations are analysed by RE, CSI and *m*-RMSE. The RE is used to

evaluate the accumulated rainfall amount, and CSI and *m*-RMSE are applied to assess the spatiotemporal distributions of the rainfall simulation.

Among the thirty-six physical parameterisation combinations, experiment 13 outperforms the other parameterisation schemes as a whole. For the accumulated rainfall simulation, experiment 13 performs the best for all the three storm events. Experiment 13 and 15 are generally the right choices for the simulations of spatial rainfall distributions. Experiment 13, 14, 15 and 16 show convincing simulations of temporal rainfall distributions. For the typhoon storm events in southeast coast of China, WSM6 for microphysics, RRTMG/RRTMG for longwave/shortwave radiation parameterisation and KF for cumulus parameterisation generally have the ability to obtain better rainfall simulations than other physical parameterisations.

The WRF model has poor capability in simulating the rainfall caused by strong convection, and the storm events with uneven distributed rainfall tend to have worse rainfall simulation in space and time dimensions. For the medium and small catchments like Meixi, the rainfall has high uncertainty, especially in space and time. Data assimilation is an efficient method to improve the rainfall simulation and radar data with high spatiotemporal resolution are suit to be assimilated by NWP system for rainfall simulation in the medium and small catchments, which is significantly important for flood forecasting and disaster early warning. Further studies should be carried out to investigate the methods to improve the ability of rainfall simulation in the study areas.

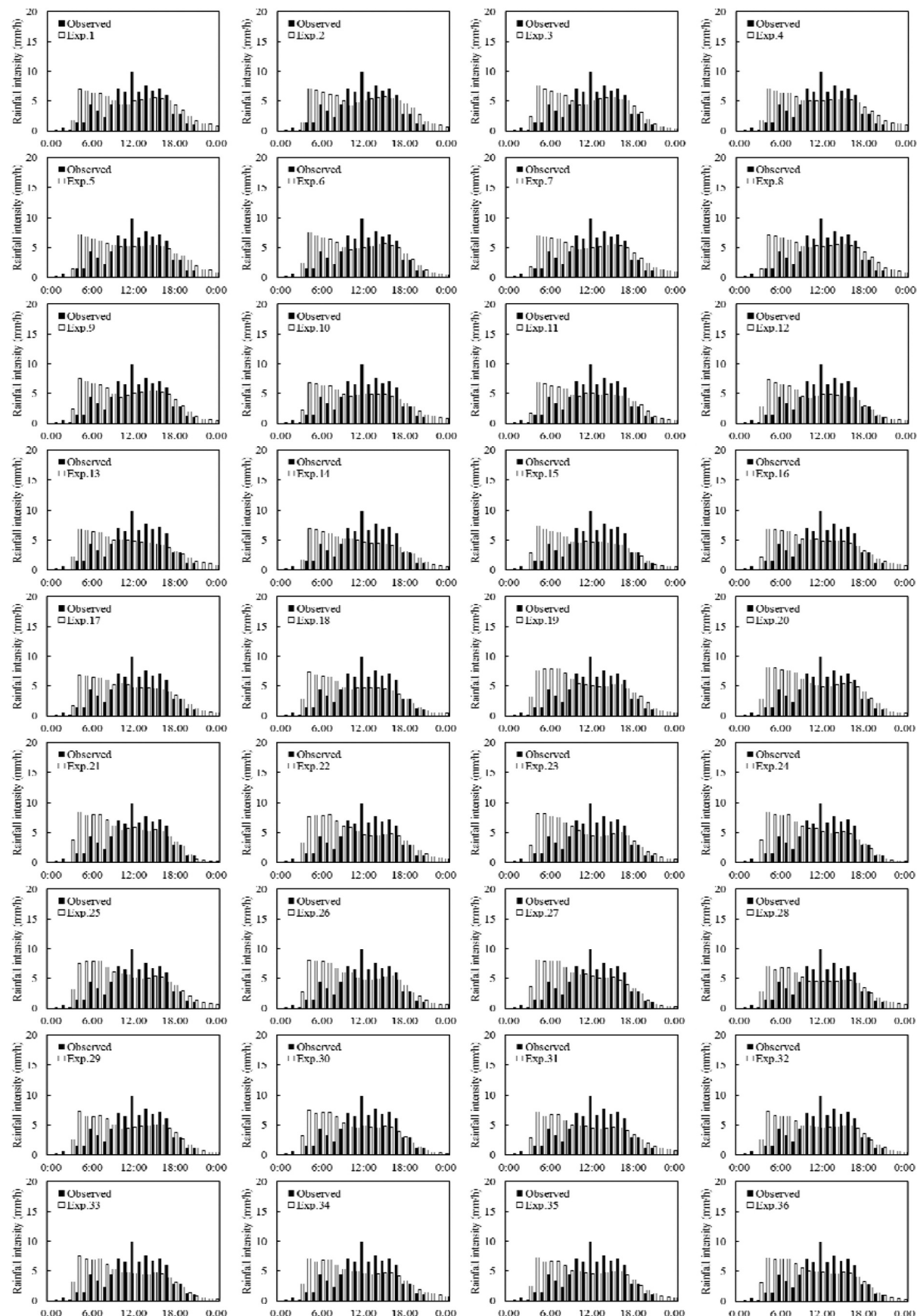


Fig. 8. Time series bars of the 36 rainfall simulations and the rainfall observation for Event I.

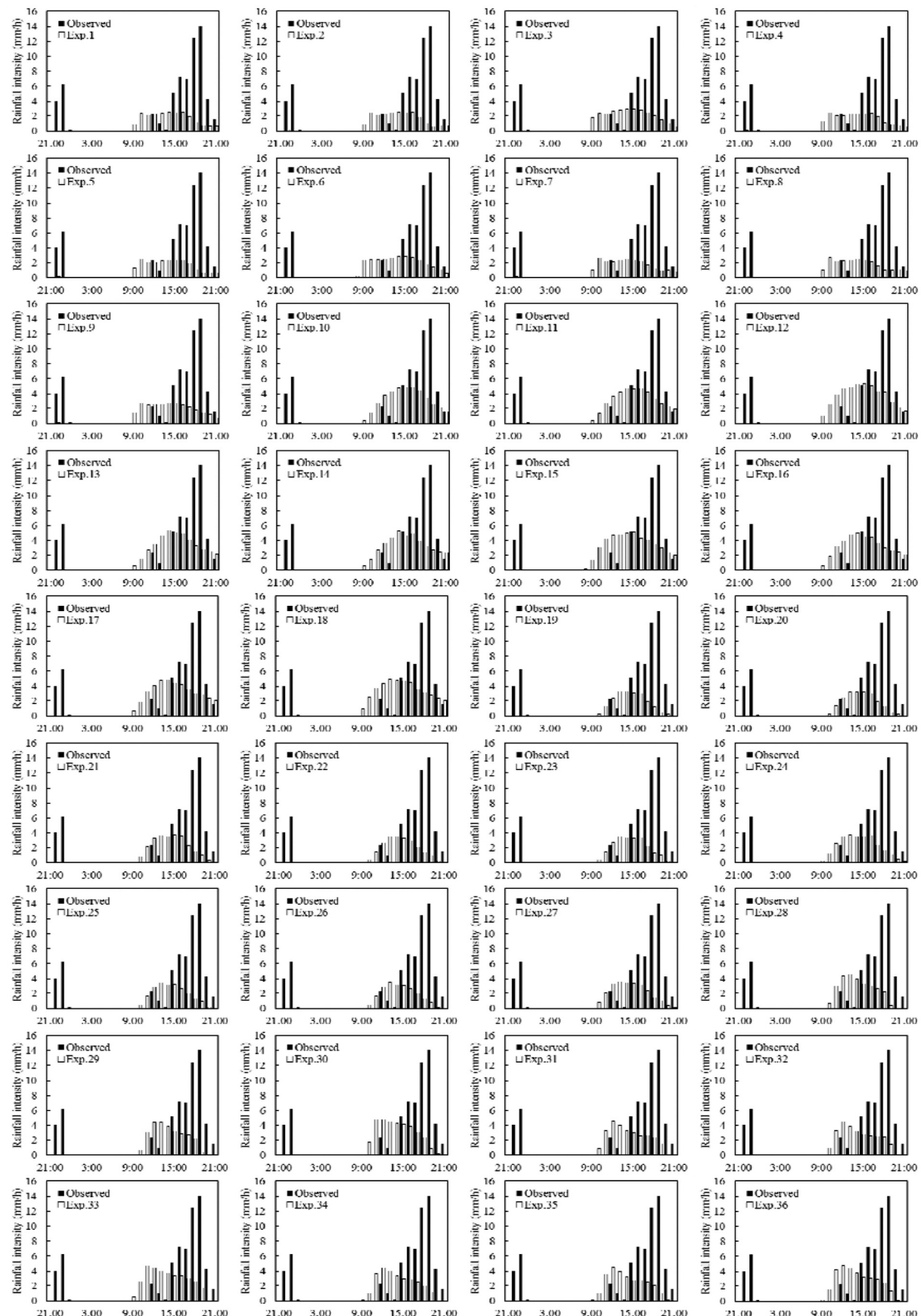


Fig. 9. Time series bars of the 36 rainfall simulations and the rainfall observation for Event II.

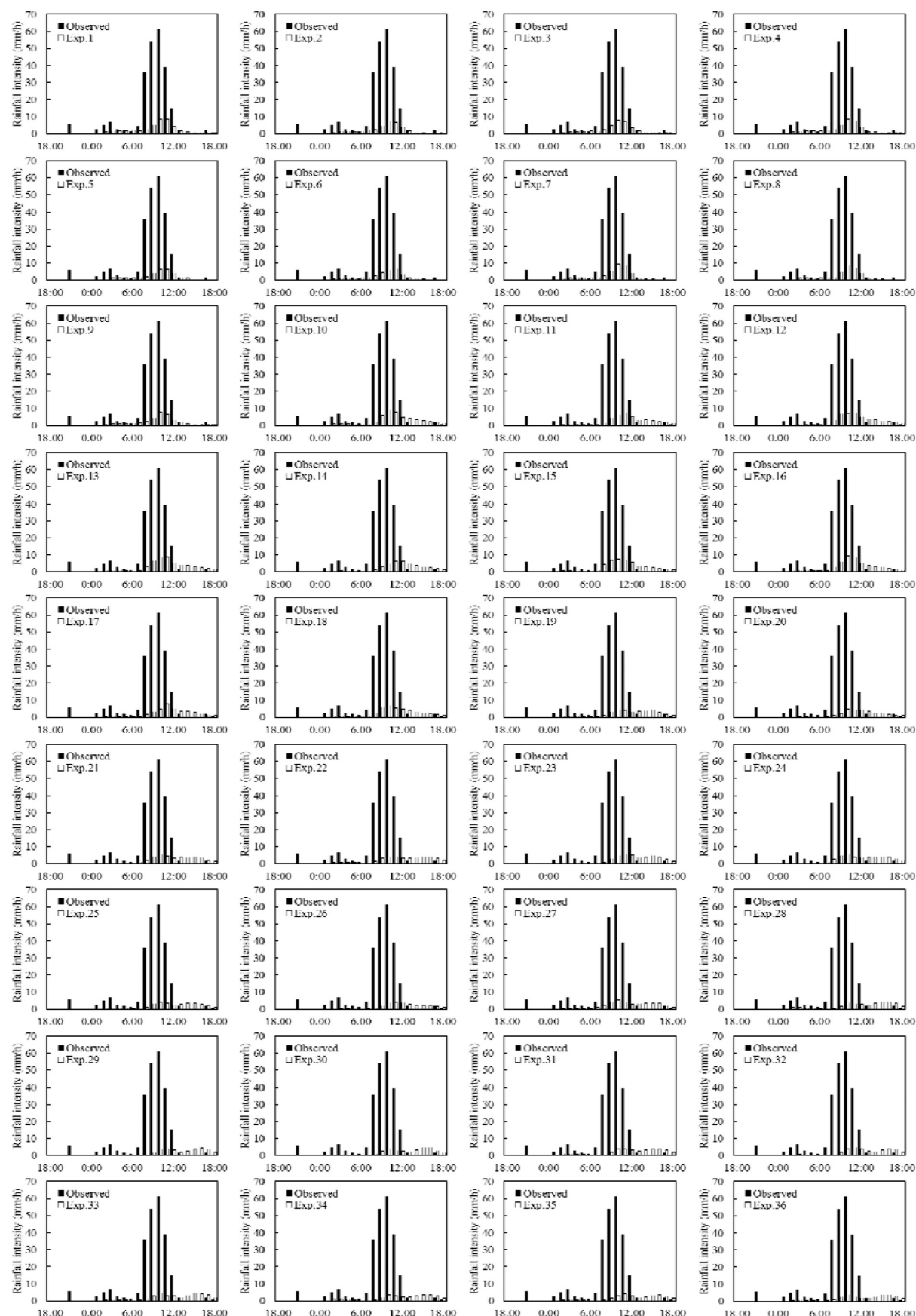


Fig. 10. Time series bars of the 36 rainfall simulations and the rainfall observation for Event III.

Table 9The average value of *CSI* and the average value of *m-RMSE* for temporal distribution of rainfall simulation.

Physical parameterisation	Event I		Event II		Event III	
	<i>CSI</i>	<i>m-RMSE</i>	<i>CSI</i>	<i>m-RMSE</i>	<i>CSI</i>	<i>m-RMSE</i>
Microphysics	WSM6	0.7144	0.6654	0.3905	1.4852	0.5952
	WDM6	0.6997	0.6633	0.3712	1.5039	0.5797
	Lin	0.7015	0.7099	0.3813	1.5105	0.5909
Longwave/shortwave radiation	RRTM/Dudhia	0.7061	0.6813	0.3750	1.5095	0.5849
	RRTMG/RRTMG	0.7092	0.6734	0.3905	1.4881	0.5954
	CAM/CAM	0.7003	0.6838	0.3776	1.5020	0.5855
Cumulus parameterisations	BMJ	0.6950	0.6746	0.3726	1.6092	0.5330
	KF	0.7354	0.6185	0.3985	1.3367	0.6147
	G3D	0.6874	0.7210	0.3579	1.5688	0.6060
	GD	0.7031	0.7040	0.3950	1.4848	0.6009

Declaration of Competing Interest

None

Acknowledgements

This study was supported by the National Key R&D Program (2019YFC1510605, 2018YFC1508105), the National Natural Science Foundation of China (Grant No. 51909274, 51822906), and IWHR Research&Development Support Program (JZ0145B032020).

References

- Ahsan, M.N., Khan, A.Q., 2013. Simulation of a flood producing rainfall event of 29 July 2010 over north-west Pakistan using WRF-ARW model. *Nat. Hazards* 69, 351–363.
- Avolio, E., Federico, S., 2018. WRF simulations for a heavy rainfall event in southern Italy: verification and sensitivity tests. *Atmos. Res.* 209, 14–35.
- Cai, Y., Lu, X., Chen, G., Yang, S., 2018. Diurnal cycles of Mei-yu rainfall simulated over eastern China: sensitivity to cumulus convective parameterization. *Atmos. Res.* 213, 236–251.
- Chen, X., Wang, Y., Zhao, K., Wu, D., 2017. A numerical study on rapid intensification of typhoon Vicente (2012) in the South China Sea. Part I: verification of simulation, storm-scale evolution, and environmental contribution. *Mon. Weather Rev.* 145, 877–898.
- Duda, J.D., Wang, X., Kong, F., Xue, M., 2014. Using varied microphysics to account for uncertainty in warm-season QPF in a convection-allowing ensemble. *Mon. Weather Rev.* 142, 2198–2219.
- Evans, J.P., Ekström, M., Ji, F., 2012. Evaluating the performance of a WRF physics ensemble over South-East Australia. *Clim. Dyn.* 39, 1241–1258.
- Ferreira, J.A., Carvalho, A.C., Carvalheiro, L., Rocha, A., Castanheira, J.M., 2014. On the influence of physical parameterisations and domains configuration in the simulation of an extreme precipitation event. *Dyn. Atmos. Oceans* 68, 35–55.
- Fierro, A., Mansell, E.R., Macgorman, D.R., Ziegler, C.L., 2013. The implementation of an Explicit charging and discharge lightning scheme within the WRF-ARW model: benchmark simulations of a continental squall line, a tropical cyclone, and a winter storm. *Mon. Weather Rev.* 141, 2390–2415.
- Gómez-Navarro, J.J., Raible, C.C., Dierer, S., 2015. Sensitivity of the WRF model to PBL parametrisations and nesting techniques: evaluation of wind storms over complex terrain. *Geosci. Model Dev.* 8, 3349–3363.
- Grell, G.A., Freitas, S.R., 2014. A scale and aerosol aware stochastic convective parameterization for weather and air quality modeling. *Atmos. Chem. Phys.* 14, 5233–5250.
- Hong, S.Y., Noh, Y., Dudhia, J., 2006. A new vertical diffusion package with an explicit treatment of entrainment processes. *Mon. Weather Rev.* 134, 2318–2341.
- Hsiao, L.F., Yang, M.J., Lee, C.S., Kuo, H.C., Shih, D.S., Tsai, C.C., Wang, C.J., Chang, L.Y., Chen, D.Y.C., Feng, L., Hong, J.S., Fong, C.T., Chen, D.S., Yeh, T.C., Huang, Y.C., Guo, W.D., Lin, G.F., 2013. Ensemble forecasting of typhoon rainfall and floods over a mountainous watershed in Taiwan. *J. Hydrol.* 506, 55–68.
- Hutchison, K.D., Iisager, B.D., Jiang, X., 2017. Quantitatively assessing cloud cover fraction in numerical weather prediction and climate models. *Rem. Sens. Lett.* 8, 723–732.
- Janjić, Z.I., 2000. Comments on “development and evaluation of a convection scheme for use in climate models”. *J. Atmos. Sci.* 57, 3686.
- Ji, F., Evans, J.P., Teng, J., Scorgie, Y., Argüeso, D., Luca, A.D., 2016. Evaluation of long-term precipitation and temperature Weather Research and Forecasting simulations for southeast Australia. *Clim. Res.* 67, 99–115.
- Kain, J.S., 2004. The Kain-Fritsch convective parameterisation: an update. *J. Appl. Meteorol.* 43, 170–181.
- Kerkhoven, E., Gan, T.Y., Shiiba, M., Reuter, G., Tanaka, K., 2005. A comparison of cumulus parameterisation schemes in a numerical weather prediction model for a monsoon rainfall event. *Hydrol. Process.* 20, 1961–1978.
- Khain, A., Lynn, B., Shpund, J., 2016. High resolution WRF simulations of Hurricane Irene: Sensitivity to aerosols and choice of microphysical schemes. *Atmos. Res.* 167, 129–145.
- Li, X., Fan, K., Yu, E., 2020. Hindcast of extreme rainfall with high-resolution WRF: model ability and effect of physical schemes. *Theor. Appl. Climatol.* 139, 639–658.
- Liguori, S., Rico-Ramirez, M.A., Schellart, A.N.A., Saul, A.J., 2012. Using probabilistic radar rainfall nowcasts and NWP forecasts for flow prediction in urban catchments. *Atmos. Res.* 103, 80–95.
- Lim, K.S.S., Hong, S.Y., 2010. Development of an effective double-moment cloud microphysics scheme with prognostic cloud condensation nuclei (CCN) for weather and climate models. *Mon. Weather Rev.* 138, 1587–1612.
- Lin, Y.L., Farley, R.D., Orville, H.D., 1983. Bulk parameterisation of the snow field in a cloud model. *J. Clim. Appl. Meteorol.* 22, 1065–1092.
- Liu, J., Bray, M., Han, D., 2012. Sensitivity of the weather research and forecasting (WRF) model to downscaling ratios and storm types in rainfall simulation. *Hydrol. Process.* 26, 3012–3031.
- Liu, J., Bray, M., Han, D., 2013. A study on WRF radar data assimilation for hydrological rainfall prediction. *Hydrol. Earth Syst. Sci.* 17, 3095–3110.
- Liu, Y., Sun, Z., Chen, M., Huang, H.L.A., Gao, W., 2018. Assimilation of atmospheric infrared sounder radiances with WRF-GSI for improving typhoon forecast. *Front. Earth Sci.* 12, 457–467.
- Madala, S., Satyanarayana, A.N.V., Rao, T.N., 2014. Performance evaluation of PBL and cumulus parameterisation schemes of WRF ARW model in simulating severe thunderstorm events over Gadanki MST radar facility - case study. *Atmos. Res.* 139, 1–17.
- Mao, J., Wu, G., 2008. Influences of Typhoon Chanchu on the 2006 South China Sea summer monsoon onset. *Geophys. Res. Lett.* 35, L12809.
- Maussion, F., Scherer, D., Finkelnburg, R., Richters, J., Yang, W., Yao, T., 2011. WRF simulation of a precipitation event over the Tibetan Plateau, China – an assessment using remote sensing and ground observations. *Hydrol. Earth Syst. Sci.* 15, 1795–1817.
- Mohan, P.R., Venkata, S.C., Yesubabu, V., Baskaran, R., Venkatraman, B., 2018. Simulation of a heavy rainfall event over Chennai in Southeast India using WRF: sensitivity to microphysics parameterisation. *Atmos. Res.* 210, 83–99.
- Mohapatra, G.N., Rakesh, V., Ramesh, K.V., 2017. Urban extreme rainfall events: categorical skill of WRF model simulations for localized and non-localized events. *Q. J. Roy. Meteor. Soc.* 147, 2340–2351.
- Montornès, A., Codina, B., Zack, J.W., 2015. Analysis of the ozone profile specifications in the WRF-ARW model and their impact on the simulation of direct solar radiation. *Atmos. Chem. Phys.* 15, 2693–2707.
- Otiemo, G., Mutemi, J.N., Opijah, F.J., Ogollo, L.A., Omondi, M.H., 2019. The sensitivity of rainfall characteristics to cumulus parameterisation schemes from a WRF model. Part I: a case study over East Africa during wet years. *Pure Appl. Geophys.* 1, 1–16.
- Patel, P., Ghosh, S., Kaganlkar, A., Islam, S., Karmakar, S., 2019. Performance evaluation of WRF for extreme flood forecasts in a coastal urban environment. *Atmos. Res.* 223, 39–48.
- Potty, J., Oo, S.M., Raju, P.V.S., Mohanty, U.C., 2012. Performance of nested WRF model in typhoon simulations over West Pacific and South China Sea. *Nat. Hazards* 63, 1451–1470.
- Ratnam, J.V., Behera, S.K., Krishnan, R., Doi, T., Ratna, S.B., 2017. Sensitivity of Indian summer monsoon simulation to physical parameterisation schemes in the WRF model. *Clim. Res.* 74, 43–66.
- Sharma, A., Fernando, H.J.S., Hamlet, A.F., Hellmann, J.J., Barlage, M., Chen, F., 2017. Urban meteorological modeling using WRF: a sensitivity study. *Int. J. Climatol.* 37, 1885–1900.
- Shen, F., Xue, M., Min, J., 2017. A comparison of limited-area 3DVAR and ETKF-En3DVAR data assimilation using radar observations at convective scale for the prediction of Typhoon Saomai (2006). *Meteorol. Appl.* 24, 628–641.
- Sivapalan, M., Blöschl, G., 1998. Transformation of point rainfall to areal rainfall: intensity-duration-frequency curves. *J. Hydrol.* 204, 150–167.
- Srivastava, P.K., Han, D., Rico-Ramirez, M.A., O'Neill, P., Islam, T., Gupta, M., Dai, Q., 2015. Performance evaluation of WRF-Noah Land surface model estimated soil

- moisture for hydrological application: synergistic evaluation using SMOS retrieved soil moisture. *J. Hydrol.* 529, 200–212.
- Sun, J., Wang, H., 2013. Radar data assimilation with WRF 4D-Var. Part II: comparison with 3D-Var for a squall line over the U.S. Great Plains. *Mon. Weather Rev.* 141, 2245–2264.
- Sun, X., Xie, L., Semazzi, F., Liu, B., 2015. Effect of lake surface temperature on the spatial distribution and intensity of the precipitation over the lake victoria basin. *Mon. Weather Rev.* 143, 1179–1192.
- Tang, J., Guo, X., Chang, Y., 2019. A numerical investigation on microphysical properties of clouds and precipitation over the Tibetan Plateau in summer 2014. *J. Meteorol. RES-PRC* 33, 463–477.
- Tian, J., Liu, J., Yan, D., Li, C., Chu, Z., Yu, F., 2017a. An assimilation test of Doppler radar reflectivity and radial velocity from different height layers in improving the WRF rainfall forecasts. *Atmos. Res.* 198, 132–144.
- Tian, J., Liu, J., Yan, D., Li, C., Yu, F., 2017b. Numerical rainfall simulation with different spatial and temporal evenness by using a WRF Multiphysics ensemble. *Nat. Hazards Earth Syst. Sci.* 17, 563–579.
- Yuan, X., Liang, X., Wood, E.F., 2011. WRF ensemble downscaling seasonal forecasts of China winter precipitation during 1982–2008. *Clim. Dyn.* 39, 2041–2058.
- Zhang, C., Wang, Y., Hamiton, K., 2011. Improved representation of boundary layer clouds over the southeast Pacific in ARW-WRF using a modified Tiedtke cumulus parameterization scheme. *Mon. Weather Rev.* 139, 3489–3513.
- Zittis, G., Hadjinicolaou, P., 2017. The effect of radiation parameterisation schemes on surface temperature in regional climate simulations over the MENA-CORDEX domain. *Int. J. Climatol.* 37, 3847–3862.